CONTRAST MEDIA & MOLECULAR IMAGING

Received: 5 October 2012, Revised: 6 June 2013, Accepted: 9 June 2013, Published online in Wiley Online Library

(wileyonlinelibrary.com) DOI: 10.1002/cmmi.1554

Influence of paramagnetic melanin on the MRI contrast in melanoma: a combined high-field (11.7 T) MRI and EPR study

Q. Godechal[a], L. Mignion[a], O. Karroum[a], J. Magat[a], P. Danhier[a], R. Morandini[b], G. E. Ghanem[b], P. Leveque[a] and B. Gallez[a]*

Melanoma is the most dangerous form of skin cancer and its incidence is rising each year. Because the current methods of diagnosis based on the visual aspect of the tumor show limitations, several new techniques are emerging to help in this diagnosis, amongst which are magnetic resonance imaging (MRI) and electron paramagnetic resonance (EPR). The origin of the typical contrast pattern observable in melanoma in T_1- and T_2-weighted images remains to be elucidated and is a source of controversy. In addition, melanin could create sufficient magnetic inhomogeneities to allow its visualization on T_2*-weighted images using high-field MRI. In order to elucidate the possible role of melanin in the MRI contrast of melanoma, the present study was designed to correlate the paramagnetic content in melanin pigment to the contrast on T_1-, T_2- and T_2*-weighted images. MR images were obtained *in vivo* at 11.7 T using four types of experimental tumors with different pigmentations (B16, HBL, LND1 melanomas and KHT sarcomas). The paramagnetic content in melanin pigment was measured by EPR. No significant correlation was observed between the content in melanin and the relaxation times T_1, T_2 and T_2*, emphasizing that the presence of pigment alone has negligible effect on the MRI contrast. Copyright © 2014 John Wiley & Sons, Ltd.

Keywords: magnetic resonance imaging; MRI; melanoma; melanin; EPR; ESR

1. INTRODUCTION

Malignant melanoma is a cancer characterized by the uncontrolled proliferation of melanocytes, mainly in skin, but also in eyes and exceptionally in several other locations such as the oral cavity, esophagus or rectum. The incidence of the cutaneous form of melanoma is constantly rising (1), and even if it represents $<5\%$ of the total of skin cancer diagnosed every year (2), it is responsible of $>75\%$ of the deaths linked to a skin cancer (3). Moreover, malignant melanoma is the second most common cancer amongst the young white population (15–29 years), after Hodgkin Lymphoma (4).

Owing to its ability to visualize subcutaneous tissues, the magnetic resonance imaging (MRI) technique has been used for a long time to aid diagnosis of skin tumors and particularly malignant melanoma. While early studies demonstrated that MRI was able to measure accurately Breslow's and Clark's index (tumor thickness and penetration) (5–7), others proved that MRI was also able to discriminate pigmented malignant melanomas from benign cutaneous pigmented lesions according to their morphological characteristics (8) or their MR contrast. For that purpose, T_2-weighted (T_2W) images were found more efficient than T_1-weighted (T_1W) images (9–11). These results were however contested in further studies where MRI was unable to discriminate benign from malignant lesions (12,13), on both T_1W and T_2W images.

The origin of the typical contrast pattern observable in melanoma (hyperintensity on T_1W and hypointensity on T_2W) remains to be elucidated and is a source of controversy. Most authors generally attribute the decrease in the relaxation times T_1 and T_2 in melanoma to the presence of melanin, a paramagnetic macromolecule synthesized within the melanocytes. The decrease in T_1 and T_2 induces a visible change of the signal intensity in melanomas compared with their close environment (subcutis for the skin melanomas, vitreous body for the uveal melanomas, cortex for cerebral metastases) (14–18). However, in some other studies, the expected pattern was found only in a small part of the melanoma tested, the others exhibiting a variable range of intensities both in T_1W and T_2W (19–22), intensities that could not always be explained by the concentration of melanin. Another possible source of contrast can rely on susceptibility effects induced by the melanin pigments. With the increasing availability of very high field MRI, we hypothesized that melanin could create sufficient magnetic inhomogeneities to allow its visualization on T_2*-weighted images (T_2*W).

In order to elucidate the possible role of melanin in the MRI contrast of melanoma, the present study was designed to correlate

* *Correspondence to: Gallez, Bernard, Louvain Drug Research Institute, Biomedical Magnetic Resonance Research Group, Université catholique de Louvain, Avenue Mounier 73.08, B-1200 Brussels, Belgium. Email: Bernard.Gallez@uclouvain.be*

a *Q. Godechal, L. Mignion, O. Karroum, J. Magat, P. Danhier, P. Leveque B. Gallez*
Biomedical Magnetic Resonance Research Group, Louvain Drug Research Institute, Université Catholique de Louvain, Avenue Mounier 73.40, 1200 Brussels, Belgium

b *R. Morandini, G. E. Ghanem*
Laboratoire d'Oncologie et de Chirurgie Expérimentale, Institut Jules Bordet, Université Libre de Bruxelles, 1 rue Heger-Bordet, 1000 Brussels, Belgium

the paramagnetic content in melanin pigment to the contrast on T_1W, T_2W and T_2*W images. We used four types of experimental tumors with different pigmentation: highly pigmented B16F10 melanoma, moderately pigmented HBL melanoma, non-pigmented LND1 melanoma and non-pigmented KHT sarcoma. The paramagnetic content in melanin pigment was measured by electron paramagnetic resonance (EPR). As shown previously, EPR spectrometry is the ideal tool to assess the concentration of paramagnetic species like melanin inside biological samples in a specific manner (23–26). The combined use of MRI and EPR on the same samples should unambiguously determine a possible relationship between the MR contrast and the concentration of melanin in the tumors.

2. RESULTS AND DISCUSSION

2.1. EPR Measurements

EPR was previously demonstrated to be an accurate method to measure the concentration of melanin within biological samples (23–26). The EPR measurements carried out in the present study were performed *ex vivo* on the tumors after the MRI examinations. The differences observed in the EPR measurements were consistent with differences in pigmentation of the tumor models. As shown in Fig. 1, the tumors from the B16F10 group, which are highly pigmented, displayed the highest signal-to-noise ratio (SNR) per unit of weight. The difference between this group and the three other groups was highly significant ($p < 0.001$). The HBL group, which was expected to be moderately pigmented, exhibited a slightly higher SNR compared with the two non-pigmented groups (KHT and LND1). This difference was significant using a *t*-test of comparison when comparing two groups, but not significant using the one-way Anova test comparing all groups. The very small EPR signal recorded for the HBL group was consistent with the direct visual observation of the tumors with an absence of pigmentation spots within the HBL samples. The assumed reason for this feature is that, like LND1 cells, HBL cells were grown in a medium poor in tyrosine, which is the key substrate for melanogenesis. As a consequence, it is likely that the cells lost the ability to synthesize melanin once injected in animals. The two other groups, KHT sarcoma and the amelanotic LND1 melanoma, displayed a low SNR, confirming the absence of pigmentation within these models. Comparison of the mean SNRs obtained from all groups and a calibration curve previously achieved for the EPR measurements of saepia melanin (24) provides an idea of the overall concentration of melanin present in each group. This was calculated at 2.93 μg/mg tissue for B16, 0.60 μg/mg tissue for HBL, 0.21 μg/mg tissue for LND1 and 0.18 μg/mg tissue for KHT. The negligible signal obtained for the two non-pigmented groups originates probably from the presence of organic free radicals, as demonstrated for several freeze-dried tissues (27). The presence of Fe^{3+} (single line at $g = 4.3$) or Mn^{2+} (six-line spectrum, $g = 2.15$ for downfield line) was also checked for each sample. Mn^{2+} was not detectable in 15 out of the 20 samples analyzed. For the other five samples, the signal was just out of the noise, and only detectable because of the particular pattern of the spectrum. Iron was detected in all samples. The mean concentration of Fe^{3+} was 0.16 μg/g (dry tissue) and ranged from 0.03 to 0.62 μg/g. Overall, these results indicate that the amount of metal ions was very low in the tumors analyzed in the present study.

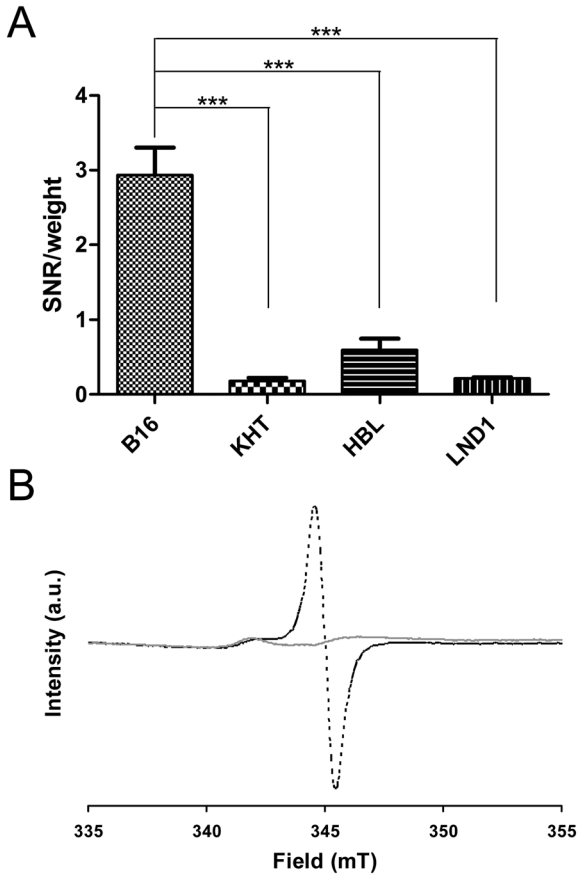

Figure 1. EPR measurements. (A) Effect of the pigmentation on the normalized electron paramagnetic resonance (EPR) intensity. The signal-to-noise ratio of the EPR spectra was normalized with the weight of the samples measured on four different tumor models. The difference between the B16 group and the three other groups was highly significant ($p < 0.001$). (B) Typical EPR spectra obtained in melanoma B16 samples (highly pigmented, black dotted line) and in melanoma LND1 samples (non pigmented, gray line).

2.2. MRI Measurements

The four tumor models were measured *in vivo* with high-field MRI (11.7 T) using T_1W, T_2W and T_2*W sequences. On the T_1W images, the contrast between the tumors and the surrounding tissues did not differ from one group to another. In each group, all tumors (pigmented or non-pigmented) were iso- to hyperintense in comparison with the muscle (Fig. 2), and when the subcutis was visible, were hypointense in comparison with the subcutis. The contrast in comparison with the muscle was expected because the muscle has a long T_1 relaxation time and low intensity on T_1W images. However, the similar appearance of the pigmented and non-pigmented tumors on T_1W images was more unexpected. Indeed, pigmented melanoma lesions were reported to exhibit a hyperintense signal on T_1W images when compared with the surrounding tissues, subcutis included (15–19) and when compared with non-pigmented tumors (7). The only notable difference between the B16 group and the others was the presence of hypointense spots visible in some tumors (3/6) of this group, as shown in Fig. 2(a). No spots could be observed in the other groups. The presence of such hypointense spots was not linked to the presence of susceptibility effects as they were not observed in the corresponding T_2*W images.

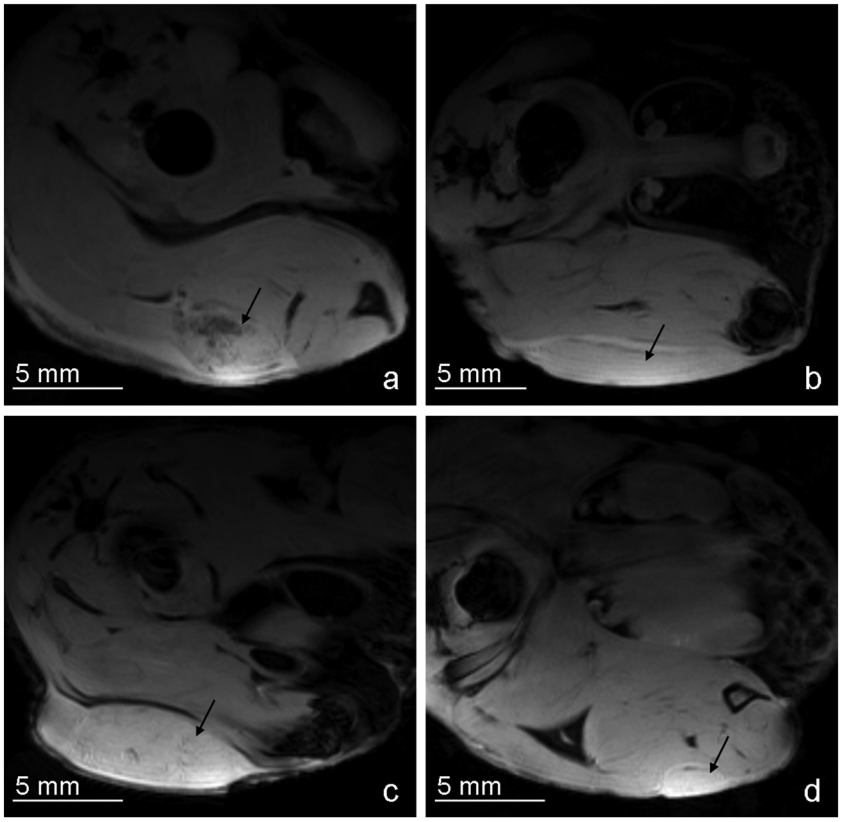

Figure 2. T_1-Weighted (T_1W) MR images. The T_1-weighted MR images of a B16 melanoma (a), KHT sarcoma (b), HBL melanoma (c) and LND1 melanoma (d) are displayed, the tumors being pointed out by an arrow. All tumors appear iso- to hyperintense in comparison to the muscle. Hypointense spots, as shown on (a) could be seen in three of the six B16 tumor. These images were acquired with $TR = 800$ ms and $TE = 2.5$ ms.

Similarly, the contrast observed on T_2W and T_2*W images did not reveal different from one group to another. On T_2W (Fig. 3) and T_2*W images (Fig. 4), all tumors appeared hyperintense in comparison to the muscle, and, when the subcutis was visible, appeared hypointense compared with the subcutis. The T_2 was measured using a multiecho sequence and this value was normalized with the T_2 measured in the muscle. This ratio was compared between the different groups by using a one-way Anova test (Fig. 5). There was no significant difference between all groups. The same result was obtained for T_2* (Fig. 6).

The results we obtained at high field are not in agreement with some previous studies done at lower magnetic field, which pointed out the efficiency of T_1W (28,29) or T_2W (30) sequences to distinguish pigmented tumors or pigmented areas from the non-pigmented ones. Still, it is interesting to note that the results obtained so far were quite controversial as studies that obtained significant results with T_1W sequences failed to observe a correlation between melanin and the T_2, and reciprocally. In addition, while several studies claimed that pigmented melanomas exhibited a typical pattern on MR images (14–18), others failed to demonstrate any correlation between the pigmentation of the tumor and the MR contrast (19–22). So far, only one *in-vitro* study correlated the MR signal intensity (T_2W images) with the concentration of melanin (31). Other studies failed to show any correlation between synthetic melanin concentration and MR contrast (32–34). Here, we used EPR spectroscopy as an accurate and sensitive measurement of the paramagnetic content in melanin pigment in the biological samples examined by MRI. We did not observe any correlation between both parameters, showing that melanin alone cannot be responsible for changes in T_1W and T_2W contrast at high field.

Interestingly, *in vitro* studies (32–34) demonstrated that, when supplemented with metal ions like Cu^{2+}, Mn^{2+} or Fe^{3+}, melanin decreased both relaxation times T_1 and T_2 proportionally to its concentration. It is noteworthy that the effects of metal ions alone on the relaxation times were significantly lower than those of the combination melanin–ions (33) and this property was recently exploited to develop a metal-based MRI sensor that reports the formation of melanin in melanoma cells (35). It seems consequently that melanin alone does not possess sufficient free radicals to induce visible effects on MR contrast and that the presence of metal ions is necessary to induce such observable effects. In the study of Enochs (32), other parameters like pH and aggregation of melanin molecules were also investigated additionally to the presence of metal ions. Although both parameters were shown to have a small influence on the MR contrast, the effect was negligible when compared with the effect of the presence of metal ions, especially Fe^{3+}. Interestingly, the effect on water relaxation of metal ions bound to melanin can be very different as a function of the structure and physical state of the pigment. Paramagnetic metal ions that are bound by melanin-chelating groups are sequestered from the solution, so their effect on water proton relaxation rates becomes very small. Other pigments that are structurally related to melanin, such as partly oxidized melanin or melanin free acids (36), are soluble, high-molecular-weight polymers. Unlike solid melanin particles, metal ions bound to such polymers show a marked effect on water proton relaxation rates. Little information is available about the final structure of melanin in melanocytes.

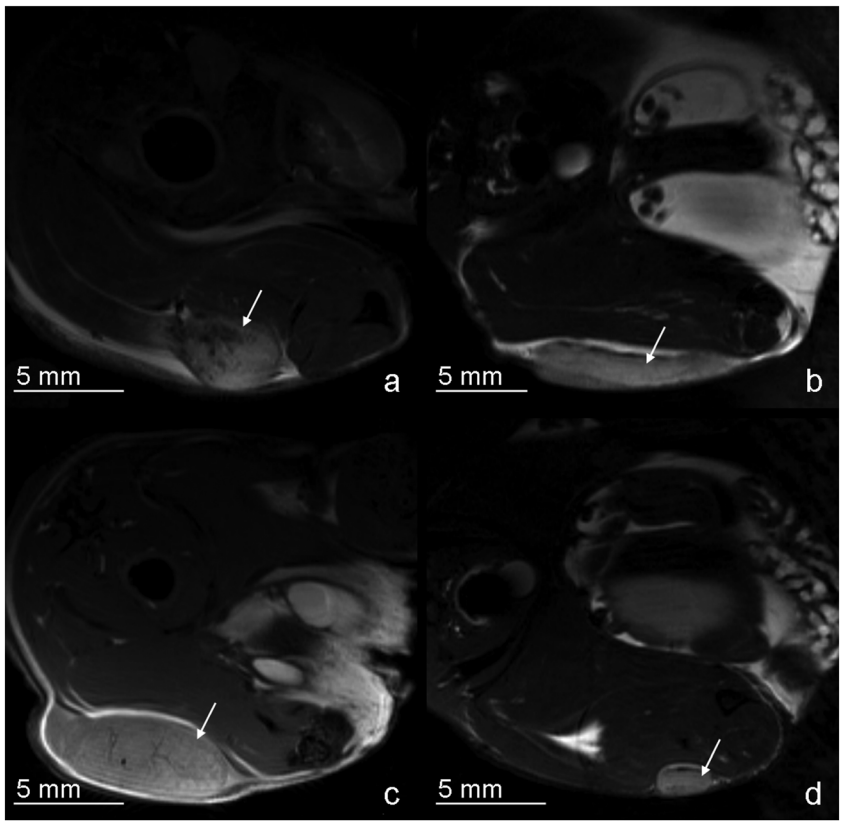

Figure 3. T_2-Weighted (T_2W) MR images. The T_2-weighted MR images of a B16 melanoma (a), KHT sarcoma (b), HBL melanoma (c) and LND1 melanoma (d) are displayed, the tumors being pointed out by an arrow. All tumors appear hyperintense in comparison to the muscle. These images were acquired with $TR = 2500$ ms and $TE = 33$ ms.

Nevertheless, the high efficiency of the photon absorption in the visible and UV, and the semiconductor properties of melanins, especially eumelanin (37), lead to the assumption that these pigments are highly polymerized structures and reside in melanocytes in the form of solid granules. This polymerized structure was first thought to be heteropolymeric (38), but a supramolecular architecture was then proposed for eumelanin particles (39) suggesting a stack aggregate ultrastructure composed of several planar sheets. Numerous studies using mass spectroscopy (40), atomic force microscopy (41) or X-ray diffraction (42) appear to support this structure. In addition, the casing model proposed by Agrup *et al*. (43) and kept up to date by Wakamatsu (44), which describes the configuration of melanin granules within the melanosome, tends to confirm the solid state of melanin molecules. A recent study from Pelès *et al*. (45) provided direct evidence that supports this casing model. Photon emission microscopy was there used to observe the surface of the substructures inside the melanosomes and revealed the presence of eumelanin granules. Overall, this aggregate structure of melanin in melanocytes together with the absence of a sufficient amount of metal ions (as measured for Fe^{3+} and Mn^{2+} in our EPR studies) seems therefore the most plausible explanation to the absence of T_1 and T_2 MRI contrast.

Finally, the influence of the presence of melanin on the T_2*W contrast appeared non-significant, indicating that, despite the use of a high magnetic field, the magnetic susceptibility of melanin was not sufficient to induce magnetic inhomogeneities within the tumors. The only study ever published attempting to correlate the presence of melanin with the T_2* MR contrast displayed evasive results. On 120 melanoma brain metastases measured with T_2*W sequences, 50 tumors exhibited a hypointense aspect. In comparison, for the same number of pulmonary carcinoma brain metastases, only 10 tumors exhibited a hypointense aspect. However, after separating the tumors into three different groups as a function of the pigmentation, the highly pigmented group did not reveal a particular hypointensity when compared with the other groups, and no correlation was found between the melanin concentration and the susceptibility effect (46). Our present results reinforce the fact that the presence of a high concentration of melanin is not sufficient to guarantee clear susceptibility effects even at high magnetic fields. Here also, the presence or absence of metal ions might be of the greatest importance in the contrast observed on MR images.

In conclusion, relaxation MR parameters cannot be considered as reliable biomarkers to assess the concentration of melanin in melanomas, and melanin alone cannot explain differences in relaxation times observed in some studies. The presence of metals is likely to play a determinant role and further *in vivo* studies investigating this particular aspect should be performed to allow a better understanding of the role played by melanin and metal ions on the MR intensity.

3. EXPERIMENTAL

3.1. Cell Cultures and Mouse Models

Four different tumor cell models were cultured, implanted and used for MRI and EPR measurements. B16F10 mouse melanoma cells were routinely cultured in DMEM-glutamax (pyruvate 1 g/l, glucose 1 g/l)

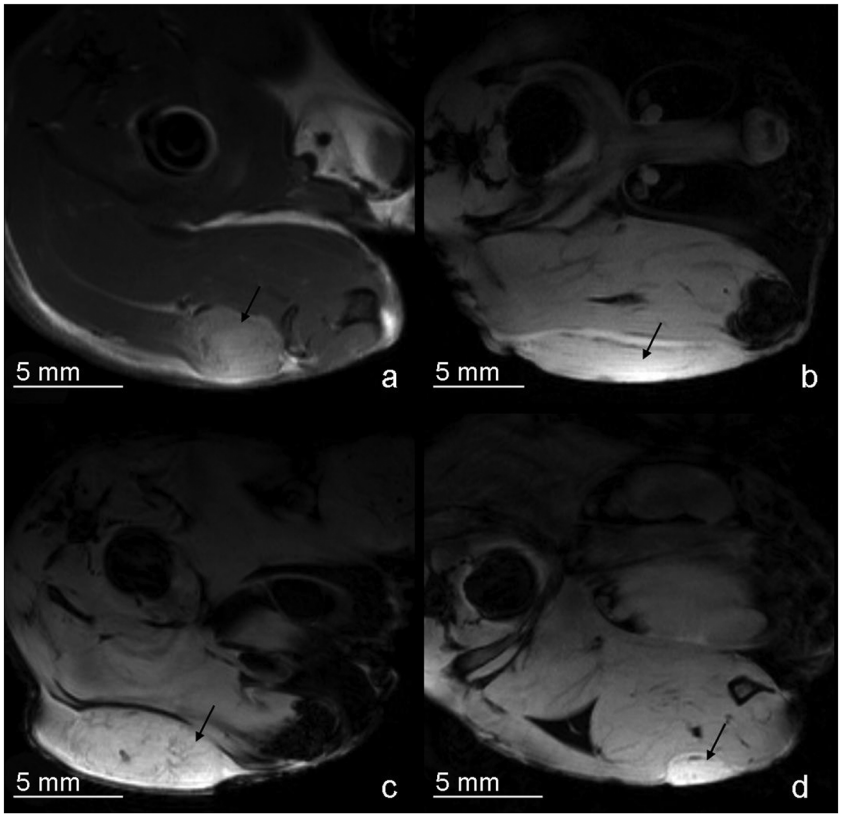

Figure 4. T_2*-Weighted MR images. The T_2*-weighted MR images of a B16 melanoma (a), KHT sarcoma (b), HBL melanoma (c) and LND1 melanoma (d) are displayed, the tumors being pointed out by an arrow. All tumors appear hyperintense in comparison to the muscle. Hypointense spots visible on T_1W and/or T_2W images are not always observable on T_2*W images. These images were acquired with $TR = 1500$ ms and $TE = 3.5$ ms.

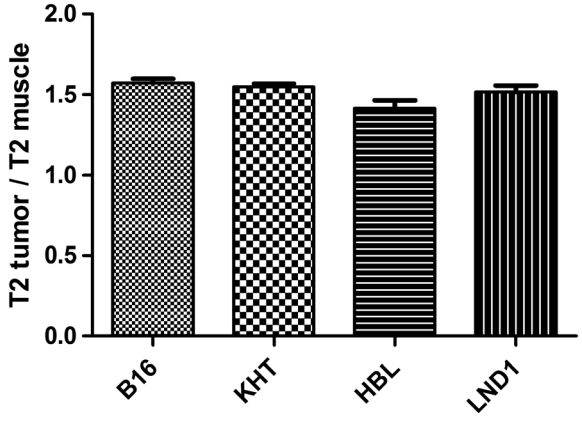

Figure 5. Measurements of the T_2 relaxation time. The relaxation time T_2 was measured for every tumor and normalized with the T_2 of the surrounding muscle. According to the one-way ANOVA test results, no significant difference could be observed between the four experimental tumor models.

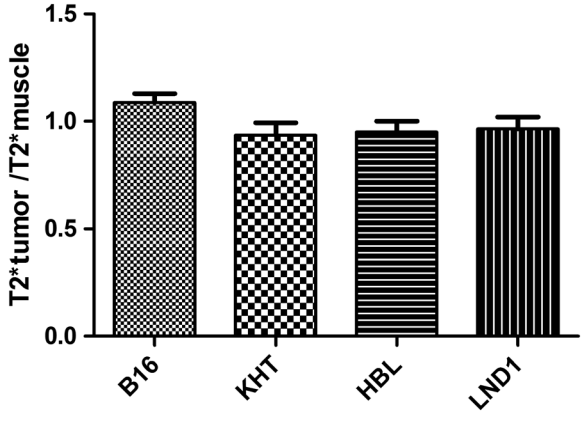

Figure 6. Measurements of the T_2* relaxation time. The relaxation time T_2* was measured for every tumor and normalized with the T_2* of the surrounding muscle. According to the one-way ANOVA test results, no significant difference could be observed between the four experimental tumor models.

medium supplemented with 10% heat-inactivated fetal bovine serum (HIFBS) and 1% penicillin–streptomycin (PS). An aliquot of 1×10^6 cells was injected subcutaneously in the left leg of 8-week-old C57BL6 mice (Elevage Janvier, France, $n = 6$). Tumors grew for 9 days before measurements. KHT mouse sarcoma cells were routinely cultured in MEM-alpha-glutamax (pyruvate 1 g/l, glucose 1 g/l) supplemented with 10% HIFBS and 1% PS. An aliquot of 1×10^6 cells was injected subcutaneously in the left leg of 8-week-old C3H mice (Elevage Janvier, France, $n = 6$). Tumors grew for 9 days before measurements. Pigmented LOCE-MM001 (known as HBL) and non-pigmented LOCE-MM011 (known as LND1) human melanoma cells were provided as a gift by Professor G. E. Ghanem from Bordet Institute, Brussels and were routinely cultured in HamF10 medium supplemented with 5% HIFBS, 5% heat-inactivated newborn calf serum (HINCS), 1% PS–glutamin and 1% kanamycin. An aliquot of 5×10^6 cells was injected subcutaneously in the left

leg of 8-week-old NMRI-nu (nu/nu) mice (Elevage Janvier, France, *n* HBL = 3, *n* LND1 = 3). Tumors grew for 21 days before measurements. For all the models, the number of cells injected and the growth period were determined to provide tumors with equivalent sizes. C57Bl6 and KHT mice were depilated 1 day before the experiment.

Mouse care and experimental procedures were approved by the local ethics committee of the Université Catholique de Louvain according to the national animal care regulations (N/ref. 2010/12AVR/120 – no. B40320108558).

3.2. Magnetic Resonance Imaging Measurements

MRI was performed with an 11.7 T, 16 cm inner diameter bore system (Bruker Biospec, Ettlingen, Germany) equipped for respiration and temperature monitoring. Mouse temperature was maintained at 37 ± 0.5°C using a water blanket connected to a circulating water bath. The system was equipped with a four-element surface coil as receiver and a 72 mm-diameter volume coil as transmitter. Two-dimensional Fast Low Angle Shot (FLASH) T_1-weighted MR sequences [repetition time (*TR*) = 800 ms, echo time (*TE*) = 2.5 ms] and Rapid Acquisition with Relaxation Enhancement (RARE) (factor 8) T_2-weighted sequences (*TR* = 2500 ms, *TE* = 33 ms) were performed perpendicularly to the cutis. The slice thickness was 1 mm and the matrix used was 256 × 256 pixels. A multislice–multiecho T_2-mapping sequence (*TR* = 2500 ms, number of echoes = 15, first *TE* = 8.62 ms, echo spacing = 8.62 ms) was performed to measure the relaxation time T_2 in a region of interest (ROI) embracing the whole tumor and in an equal-size ROI placed on the leg muscle, serving as a reference. In the same way, a multigradient-echo T_2*-mapping sequence (*TR* = 1500 ms, number of echoes = 6, first *TE* = 3.5 ms, echo spacing = 5 ms) was performed to measure the relaxation time T_2* in the tumor and the leg muscle. For each tumor, T_2 and T_2* relaxation times were calculated as the mean of the T_2 and T_2* measured on two different slices separated by 1 mm distance. The relaxation times were calculated using the Bruker ISA tool.

3.3. Electron Paramagnetic Resonance Measurements

Tumors were freeze-dried prior to EPR manipulations to avoid the non-resonant absorption of microwaves by water and increase the sensitivity of the measurements. EPR spectra were recorded at room temperature on a Bruker E540 Elexsys system (Bruker Biospin, GmBh) equipped with a Super High Sensitivity Probe (10 mm diameter, 30 mm long) operating in X-band mode at approximately 9.5 GHz and 100 kHz modulation frequency. For melanin measurements, parameters were chosen to provide the best SNR with no distortion of the signal shape. The following parameters were used: microwave power, 3.2 mW; modulation amplitude, 0.25 mT; conversion time, 10.24 ms; time constant, 5.12 ms; sweep width, 100 G; number of points, 1024; number of scans, 5; sweep time, 35 s. The intensity of the spectra was measured as the peak-to-peak amplitude of the EPR signal of melanin and was normalized to the post-freeze-drying weight of the tumors. To guarantee the integrity of the results, spectra intensities were normalized by comparison with the EPR intensity of a DPPH standard spectrum acquired between every series of measurements.

3.3.1. Iron quantification

Iron standards were prepared from solutions of $FeCl_3.6H_2O$ (UCB, Belgium), ranging from 0.25 to 2% w/v in water. Twenty-five microliters of each solution were placed on an inert support, evaporated to dryness, placed in a quartz tube and measured in X band with the following parameters: power, 20 mW; gain, 60 db; conversion time, 10.24 ms; time constant, 20.48 ms; amplitude modulation, 1 mT; center field, 163.0 mT; sweep width, 80 mT. Ten scans were acquired for each sample. The intensity of the spectra was measured as the peak-to-peak amplitude of the EPR signal. Limits of detection and quantitation using this procedure were 0.016 and 0.053 mg of Fe^{3+}, respectively.

3.4. Statistics

EPR results are given as means ± SE values from *n* animals. Comparisons between groups were performed with a one-way ANOVA test comparing all pairs of columns. *p*-Values < 0.05 (*), < 0.01 (**) or < 0.001 (***) were considered significant.

Acknowledgments

This work was supported by grants from the Belgian National Fund for Scientific Research, the Televie, the Fonds Joseph Maisin, the 'Actions de Recherches Concertées-Communauté Française de Belgique-ARC 09 /14-020' and the Fondation contre le Cancer.

REFERENCES

1. Linos E, Swetter SM, Cockburn MG, Colditz GA, Clarke CA. Increasing burden of melanoma in the United States. J Invest Dermatol 2009; 129: 1666–1674.
2. Altekruse SF, Kosary CL, Krapcho M, Neyman N, Aminou R, Waldron W, Ruhl J, Howlader N, Tatalovich Z, Cho H, Mariotto A, Eisner MP, Lewis DR, Cronin K, Chen HS, Feuer EJ, Stinchcomb DG, Edwards BK (eds). SEER Cancer Statistics Review, 1975–2007. National Cancer Institute: Bethesda, MD. Available from: http://seer.cancer.gov/csr/1975_2007/, based on November 2009 SEER data submission, posted to the SEER web site, 2010.
3. Jerant AF, Johnson JT, Sheridan CD, Caffrey TJ. Early detection and treatment of skin cancer. Am Fam Physician 2000; 62(2): 357–368.
4. Bleyer A, O'Leary M, Barr R, Ries LAG (eds). Cancer Epidemiology in Older Adolescents and Young Adults 15 to 29 Years of Age, Including SEER Incidence and Survival:1975–2000. National Cancer Institute: Bethesda, MD, 2006.
5. Zemtsov A, Lorig R, Ng TC, Xue M, Bailin PL, Bergfeld WF, Larson K, Yetman R. Magnetic resonance imaging of cutaneous neoplasms: clinicopathologic correlation. J Dermatol Surg Oncol 1991; 17(5): 416–422.
6. Ono I, Kaneko F. Magnetic resonance imaging for diagnosing skin tumors. Clin Dermatol 1995; 13(4): 393–399.
7. el Gammal S, Hartwig R, Aygen S, Bauermann T, el Gammal C, Altmeyer P. Improved resolution of magnetic resonance microscopy in examination of skin tumors. J Invest Dermatol 1996; 106(6): 1287–1292.
8. Zemtsov A, Lorig R, Bergfield WF, Bailin PL, Ng TC. Magnetic resonance imaging of cutaneous melanocytic lesions. J Dermatol Surg Oncol 1989; 15(8): 854–858.
9. Schwaighofer BW, Fruehwald FX, Pohl-Markl H, Neuhold A, Wicke L, Landrum WL. MRI evaluation of pigmented skin tumors: preliminary study. Invest Radiol 1989; 24(4): 289–293.
10. Takahashi M, Kohda H. Diagnostic utility of magnetic resonance imaging in malignant melanoma. J Am Acad Dermatol 1992; 27(1): 51–54. [Erratum in J Am Acad Dermatol 1993;28(3):513–515.]
11. Mäurer J, Knollmann FD, Schlums D, Garbe C, Vogl TJ, Bier J, Felix R. Role of high-resolution magnetic resonance imaging for differentiating melanin-containing skin tumors. Invest Radiol 1995; 30(11): 638–643.
12. Mäurer J, Schlums D, Knollmann FD, Garbe C, Vogl TJ, Bier J, Felix R. Failure of gadopentetate dimeglumine-enhanced, high-resolution magnetic resonance imaging to differentiate among melanin-containing skin tumors. Acad Radiol 1996; 3(3): 186–191.

13. Mäurer J, Hoffmann KT, Lissau G, Schlums D, Felix R. High-resolution magnetic resonance imaging for determination of thickness and depth of invasion of skin tumours. Acta Derm Venereol 1999; 79(6): 478–479.
14. Peyster RG, Augsburger JJ, Shields JA, Hershey BL, Eagle R Jr, Haskin ME. Intraocular tumors: evaluation with MR imaging. Radiology 1988; 168(3): 773–779.
15. Atlas SW, Grossman RI, Gomori JM, Guerry D, Hackney DB, Goldberg HI, Zimmerman RA, Bilaniuk LT. MR imaging of intracranial metastatic melanoma. J Comput Assist Tomogr 1987; 11(4): 577–582.
16. Isiklar I, Leeds NE, Fuller GN, Kumar AJ. Intracranial metastatic melanoma: correlation between MR imaging characteristics and melanin content. Am J Roentgenol 1995; 165(6): 1503–1512.
17. Mafee MF, Peyman GA, Grisolano JE, Fletcher ME, Spigos DG, Wehrli FW, Rasouli F, Capek V. Malignant uveal melanoma and simulating lesions: MR imaging evaluation. Radiology 1986; 160(3): 773–780.
18. Chambers RB, Davidorf FH, McAdoo JF, Chakeres DW. Magnetic resonance imaging of uveal melanomas. Arch Ophthalmol 1987; 105(7): 917–921.
19. Marx HF, Colletti PM, Raval JK, Boswell WD Jr, Zee CS. Magnetic resonance imaging features in melanoma. Magn Reson Imag 1990; 8(3): 223–229.
20. Bloom PA, Ferris JD, Laidlaw DA, Goddard PR. Magnetic resonance imaging: diverse appearances of uveal malignant melanomas. Arch Ophthalmol 1992; 110(8): 1105–1111.
21. Iyer SB, Goldberg HI, Benz CC. Magnetic resonance imaging of implanted melanomas before and after chemotherapy. Relation to ^{31}P magnetic resonance spectroscopy and tumor histology. Invest Radiol 1990; 25(10): 1076–1084.
22. Ferris JD, Bloom PA, Goddard PR, Collins C. Quantification of melanin and iron content in uveal malignant melanomas and correlation with magnetic resonance image. Br J Ophthalmol 1993; 77(5): 297–301.
23. Vanea E, Charlier N, Dewever J, Dinguizli M, Feron O, Baurain JF, Gallez B. Molecular electron paramagnetic resonance imaging of melanin in melanomas: a proof-of-concept. NMR Biomed 2008; 21(3): 296–300.
24. Godechal Q, Defresne F, Danhier P, Leveque P, Porporato PE, Sonveaux P, Baurain JF, Feron O, Gallez B. Assessment of melanoma extent and melanoma metastases invasion using electron paramagnetic resonance and bioluminescence imaging. Contrast Media Mol Imag 2011; 6(4): 282–288.
25. Godechal Q, Gallez B. The contribution of electron paramagnetic resonance to melanoma research. J Skin Cancer 2011; 273280; epub 20 September 2011.
26. Godechal Q, Leveque P, Marot L, Baurain JF, Gallez B. Optimization of electron paramagnetic resonance imaging for visualization of human skin melanoma in various stages of invasion. Exp Dermatol 2012; 21(5): 341–346.
27. Swartz HM, Molenda RP. Electron spin resonance characteristics of some normal tissues: effect of the microwave power. Science 1965; 148(3666): 94–95.
28. Atlas SW, Braffman BH, LoBrutto R, Elder DE, Herlyn D. Human malignant melanomas with varying degrees of melanin content in nude mice: MR imaging, histopathology, and electron paramagnetic resonance. J Comput Assist Tomogr 1990; 14(4): 547–554.
29. Premkumar A, Marincola F, Taubenberger J, Chow C, Venzon D, Schwartzentruber D. Metastatic melanoma: correlation of MRI characteristics and histopathology. J Magn Reson Imag 1996; 6(1): 190–194.
30. DeJordy JO, Bendel P, Horowitz A, Salomon Y, Degani H. Correlation of MR imaging and histological findings in mouse melanoma. J Magn Reson Imag 1992; 2(6): 695–700.
31. Seiler T, Bende T, Schilling A, Wollensak J. Magnetic resonance tomography in ophthalmology. I. Choroid melanoma. Klin Monbl Augenheilkd 1987; 191(3): 203–210.
32. Enochs WS, Hyslop WB, Bennett HF, Brown RD 3rd, Koenig SH, Swartz HM. Sources of the increased longitudinal relaxation rates observed in melanotic melanoma. An in vitro study of synthetic melanins. Invest Radiol 1989; 24(10): 794–804.
33. Aime S, Fasano M, Terreno E, Sarzanini C, Mentasti E. An NMR study of the interaction between melanin free acid and Mn2+ ions as a model to mimic the enhanced proton relaxation rates in melanotic melanoma. Magn Reson Imag 1991; 9(6): 963–968.
34. Tosk JM, Holshouser BA, Aloia RC, Hinshaw DB Jr, Hasso AN, MacMurray JP, Will AD, Bozzetti LP. Effects of the interaction between ferric iron and L-dopa melanin on T_1 and T_2 relaxation times determined by magnetic resonance imaging. Magn Reson Med 1992; 26(1): 40–45.
35. Szabó I, Crich SG, Alberti D, Kálmán FK, Aime S. Mn loaded apoferritin as an MRI sensor of melanin formation in melanoma cells. Chem Comm (Camb) 2012; 48(18): 2436–2438.
36. Ghiani S, Baroni S, Burgio D, Digilio G, Fukuhara M, Martino P, Monda K, Nervi C, Kiyomine A, Aime S. Characterization of human hair melanin and its degradation products by means of magnetic resonance techniques. Magn Reson Chem 2008; 46(5): 471–479.
37. McGiness JE. Amorphous semiconductor switching in melanins. Science 1974; 183: 853–855.
38. Longuet-Higgins HC. On the origin of the free radical properties of melanin. Arch Biochim Biophys Acta 1960; 186: 231–232.
39. Cheng J, Moss SC, Eisner M, Zschack P. X-ray characterization of melanins – II. Pigment Cell Res 1994; 7(4): 263–273.
40. Pezzella A, Napolitano A, d'Ischia M, Prota G, Seraglia R, Traldi P. Structural analysis of synthetic melanins from 5,6-dihydroxyindole by matrix-assisted laser desorption/ionization mass spectrometry. Rapid Commun Mass Spectrom 1997; 11: 368–372.
41. Liu Y, Simon JD. Isolation and biophysical studies of natural eumelanins: applications of imaging technologies and ultrafast spectroscopy. Pigment Cell Res 2003; 16: 606–618.
42. Capozzi V, Perna G, Carmone P, Gallone A, Lastella M, Mezzenga E, Quartucci G, Ambrico M, Augelli V, Biagi PF, Ligonzo T, Minafra A, Schiavulli L, Pallara M, Cicero R. Optical and photoelectronic properties of melanin. Thin Solid Films 2006; 511–512: 362–366.
43. Agrup, G., Hansson, C., Rorsman, H., and Rosengren, E. The effect of cysteine on oxidation of tyrosine, dopa, and cysteinyldopas. Arch Dermatol Res 1982; 272: 103–115.
44. Wakamatsu K, Ohtara K, Ito S. Chemical analysis of late stages of pheomelanogenesis: conversion of dihydrobenzothiazine to a benzothiazole structure. Pigment Cell Melanoma Res 2009; 22: 474–496.
45. Pelès, DN, Simon JD. Challenges in applying photoemission electron microscopy to biological systems. Photochem Photobiol 2009; 85: 8–20.
46. Gaviani P, Mullins ME, Braga TA, Hedley-White ET, Halpern EF, Schaefer PS, Henson JW. Improved detection of metastatic melanoma by T2*-weighted imaging. Am J Neuroradiol 2006; 27(3): 605–608.